Arab J Sci Eng (2014) 39:1271–1290
DOI 10.1007/s13369-013-0659-1

RESEARCH ARTICLE - MECHANICAL ENGINEERING

Neural Network Based Analyses for the Determination of Evaporation Heat Transfer Characteristics During Downward Flow of R134a Inside a Vertical Smooth and Corrugated Tube

M. Balcilar · A. S. Dalkilic · K. Aroonrat · S. Wongwises

Received: 24 April 2011 / Accepted: 4 July 2013 / Published online: 5 September 2013

Abstract The heat transfer characteristics of the refrigerant HFC–134a are investigated, such as convective heat transfer coefficient and pressure drop during evaporation inside a vertical smooth and five pieces of corrugated tube, using experimental data with the aim of numerically determining the best artificial intelligence method. The double tube test sections are 0.5 m long with refrigerant flowing in the inner tube and heating water flowing in the annulus. Input of the ANNs are the 14 numbers of dimensional and dimensionless values of test section, such as mass flux, heat flux, temperature difference between the tube wall and saturation temperature, average vapour quality, evaporating temperature, two-phase friction factor, two-phase multiplier, liquid and vapour Reynolds numbers, Bond number, Froude number, Weber number, depth of corrugation and helix angle for the tested corrugated tubes, whereas the outputs of the ANNs are the experimental condensation heat transfer coefficient and measured pressure drop from the analysis. The evaporation heat transfer characteristics of R134a are modelled to decide the best approach, using several ANN methods such as multi layer perceptron (MLP) and radial basis networks (RBFN). The performance of the method of MLP with 10-5-1 architecture and RBFNs with the spread coefficient of 100,000 and a hidden layer neuron number of 200 were found to be in good agreement, predicting the evaporation heat transfer coefficient and pressure drop. Dependency of outputs of the ANNs from input values is investigated and new ANN-based heat transfer coefficient correlations are developed as a result of the analyses.

Keywords Evaporation · Boiling · Heat transfer coefficient · Pressure drop · Modeling · Neural network

M. Balcilar
Computer Engineering Department,
Yildiz Technical University, 34220 Davutpasa,
Esenler, Istanbul, Turkey

A. S. Dalkilic (✉)
Heat and Thermodynamics Division,
Department of Mechanical Engineering,
Yildiz Technical University, Yildiz,
Besiktas, Istanbul 34349, Turkey
e-mail: dalkilic@yildiz.edu.tr

K. Aroonrat · S. Wongwises (✉)
Fluid Mechanics, Thermal Engineering
and Multi phase Flow Research Lab. (FUTURE),
Department of Mechanical Engineering,
Faculty of Engineering, King Mongkut's
University of Technology Thonburi, Bangmod,
Bangkok 10140, Thailand
e-mail: somchai.won@kmutt.ac.th

الخلاصة

تم التحقيق في خصائص نقل الحرارة لمبرد HFC-134a، مثل معامل انتقال الحمل الحراري وانخفاض الضغط في أثناء التبخر داخل تمليس عمودي وخمس قطع من أنبوب مموج، وذلك باستخدام البيانات التجريبية بهدف تحديد - عدديا - أفضل طريقة ذكاء اصطناعي ، وكان طول أقسام أنبوب الاختبار المزدوج 0.5 م مع تدفق المبردات في الأنبوب الداخلي وتسخين المياه المتدفقة في الحلقة ، ومدخلات الشبكات العصبية الصناعية هي 14 رقما من قيم بعدية وغير بعدية لمقطع الاختبار للأنابيب المموجة التي تم اختبارها، مثل التدفق الشامل، والتدفق الحراري، والفرق في درجة الحرارة بين جدار الأنبوب ودرجة الحرارة التشبع، ومتوسط جودة البخار، ودرجة حرارة التبخير، ومعامل الاحتكاك ذي مرحلتين، والمضاعف ذي مرحلتين ، وأرقام رينولدز للسائل والبخار، وعدد بوند، وعدد فرويد، وعدد

ويبر، وعمق التمويج وزاوية اللولب، في حين أن مخرجات الشبكات العصبية الصناعية هي معامل انتقال حرارة التكثيف التجريبي وهبوط الضغط المقاس من التحليل. وقد تمت نمذجة خصائص نقل حرارة التبخر ل R134a لتحديد أفضل نهج، وذلك باستخدام عدة أساليب ANN مثل مستقبلات الطبقة المتعددة (MLP) وشبكات القاعدة الشعاعية (RBFN)، ووجد أن أداء طريقة MLP مع هندسة معمارية 1-5-10 وRBFNs مع معامل انتشار خلايا عصبيه بمقدار 100،000 وعدد خلايا عصبية لطبقة مخفية مقداره 200 هو في اتفاق جيد، ويتوقع معامل انتقال حرارة التبخر وانخفاض الضغط ، وتم التحقيق في اعتمادية مخرجات الشبكات العصبية الصناعية على قيم الإدخال، وطورت معاملات ارتباط نقل حرارة جديدة على أساس ANN كنتيجة للتحليلات.

Abbreviations

A	Surface area, m^2
ANFIS	Adaptive neuro–fuzzy inference system
ANN	Artificial neural network
Bo	Bond number
CHF	Critical heat flux
c_p	Specific heat, J kg^{-1} K^{-1}
d	Internal tube diameter, m
E	Error
EHD	Electro hydrodynamic
f	Friction factor
Fr	Froude number
G	Mass flux, kg m^{-2} s^{-1}
GA	Genetic algorithm
GRNN	Generalized regression neural network
h	Heat transfer coefficient, W m^{-2} K^{-1}
HFC	Hydro fluorocarbons
I	Input
i	Enthalpy, J kg^{-1}
i_{fg}	Latent heat of condensation, J kg^{-1}
k	Thermal conductivity, W m^{-1} K^{-1}
L	Length of test tube, m
m	Mass flow rate, kg s^{-1}
MLP	Multi-layer perception
N	Element number
N_i^j	ith Neuron of jth hidden layer
O	Output
P	Pressure, N m^{-2}
ΔP	Pressure drop, N m^{-2}
R	Refrigerant
Re	Reynolds number
RBFN	Radial basis networks
S	Slip ratio
sp	Spread coefficient
Q	Heat transfer rate, W
q	Heat flux, kW m^{-2}
T	Temperature, °C
ΔT	Temperature difference, K
x	Average vapor quality
X_{tt}	Lockhart–Martinelli parameter
We	Weber number

Greek Symbols

φ_l^2	Two-phase multiplier
α	Void fraction
ρ	Density, kg m^{-3}
μ	Dynamic viscosity, kg m^{-1} s^{-1}
σ	Surface tension, N m^{-1}

Subscripts

avg	Average
calc	Calculated
eq	Equivalent
exp	Experimental
F	Frictional term
g	Gas/vapor
G	Gravitational term
i	Number of test data
in	Inlet
l	Liquid
M	Momentum term
ph	Preheater
o	Outlet
ref	Refrigerant
sat	Saturation
TS	Test section
tp	Two-phase
w	Water
wi	Wall inside

1 Introduction

The thermal performance of heat transfer equipment can be improved using heat transfer enhancement techniques. The rough surface technique is one of them that usually involves surface modification to promote turbulent flow and increases the heat transfer surface area. Normally, smooth tubes are replaced by corrugated tubes in many heat exchangers to increase the heat transfer rate by mixing and also limiting the fluid boundary layers close to the heat transfer surfaces. Moreover, they can promote two-phase heat transfer enhancement. Some of works regarding the heat transfer and flow characteristics of corrugated tubes are summarised below.

Nozu et al. [1,2] investigated local heat transfer and pressure gradients in pure R-114, R-113 and a zeotropic refrigerant mixture during condensation in a tube-in-tube heat exchanger. The results showed that the frictional pressure gradient data and measured heat transfer data were approximately 11 and 13 %, respectively. Dong et al. [3] investigated turbulent friction and heat transfer characteristics of four spirally corrugated tubes with various geometrical parameters. Water and oil were used as the working fluid. Their results

showed that the heat transfer coefficient enhancement varied from 30 to 120 %, while the friction factor increased from 60 to 160 % when compared with a smooth tube. One of most productive studies has been performed by Zimparov [4]. The heat transfer enhancement of a combination of three-start spirally corrugated tubes with a twisted tape was investigated. Two three-start spirally corrugated tubes combined with five twisted tape inserts with different relative pitches were employed as the test section. The results showed that the friction factor and heat transfer coefficients of three-start spirally corrugated tubes with a twisted tape were significantly higher than those of a smooth tube under the same operating conditions. Zimparov [5] presented the heat transfer enhancement using a combination of single-start spirally corrugated tubes with a twisted tape. The friction factors and inside heat transfer coefficients obtained from these tubes were higher than those obtained from the smooth tube under the same conditions. In addition, Zimparov [6,7] applied a simple mathematical model to predict the friction factors and heat transfer coefficients in a spirally corrugated configuration combined with twisted tape inserts flowing in the turbulent flow regime. The calculated friction factors and heat transfer coefficients were compared with the experimental data. The results showed that the agreement between the predicted and experimental data was fairly good.

Existing numerical studies on the subject of in-tube evaporation and boiling in the literature are summarised briefly in the following paragraphs.

Nafey [8] proposed a new method using artificial neural networks (ANN) to predict the critical heat flux (CHF) for a steam–water mixture flowing in pipes. The testing processes is performed by means of a large volume of experimental data. The algorithm of Levenberg–Marquardt was used in the analysis of ANN. Accuracy of the validation was good and a new correlation was proposed to determine the CHF. Wang et al. [9] developed a generalised neural network correlation for boiling heat transfer coefficient of R22 and its alternative refrigerants R134a, R407C and R410A, inside horizontal smooth tubes. The input of the neural network analysis was selected from four kinds of dimensionless parameter groups while the Nusselt number was used as the output. As a result of the analysis, the input parameter group based on the Gungor–Winterton correlation was found to be better than the other three groups. Scalabrin et al. [10] investigated the flow boiling inside horizontal smooth tubes for mixtures and proposed a new modelling method based on ANN for heat transfer. They extended their former study [11], which was about the same topic using pure fluids in smooth tubes, to mixtures. Their new numerical method was stated to be better than the conventional methods with regard to its accuracy. Wongwises and Disawas [12] experimentally investigated the two-phase heat transfer coefficient characteristics of HFC-134a evaporating under forced flow conditions inside a smooth horizontal tube. Different from most previous studies, the present experiments have been performed with lubricating oil in the refrigerant loop at high flow rate and high heat flux conditions. The effects of heat flux, mass flux, evaporation pressure and lubricating oil on the convection heat transfer coefficients were discussed. Sripattrapan and Wongwises [13] presented the results of simulations using a two-phase separated flow model to study the heat transfer and flow characteristics of refrigerants during evaporation in a horizontal tube. A one-dimensional annular flow model of the evaporation of refrigerants under constant heat flux was developed. Their proposed model is used to predict the variation of the temperature, heat transfer coefficient and pressure drop of various pure refrigerants flowing along a horizontal tube. Wongwises and Polsongkram [14] investigated the two-phase heat transfer coefficient and pressure drop of HFC-134a during evaporation inside a smooth, helically coiled concentric tube-in-tube heat exchanger. New correlations for the convection heat transfer coefficient and pressure drop were proposed for practical applications. Kaew-On and Wongwises [15] investigated the evaporation heat transfer coefficient and pressure drop of R-410A flowing through a horizontal aluminium rectangular multiport mini-channel of 3.48 mm hydraulic diameter. Their analysis showed that the average heat transfer coefficient of R-410A during evaporation tended to increase with increasing average quality, mass flux and heat flux, but tended to decrease with increasing saturation temperature. The pressure drop increased with increasing the mass flux, but decreased with increasing the saturation temperature, and the heat flux has no significant effect on the pressure drop. Posew et al. [16] investigated the heat transfer enhancement using the electrohydrodynamic (EHD) technique during evaporation inside horizontal smooth and micro-fin tubes. The test section was a counter-flow concentric tube-in-tube heat exchanger with R-134a flowing inside the inner tube and heating water flowing in the annulus. The maximum heat transfer enhancement ratios were 1.25 and 1.15 for smooth tube and micro-fin tube, respectively. Laohalertdecha and Wongwises [17] investigated the effects of corrugation pitch on the evaporation of R-134a flowing inside horizontal corrugated tubes. The effects of average vapour quality, equivalent Reynolds number and corrugation pitch were discussed. Differently from most previous studies, Aroonrat and Wongwises [18] studied the heat transfer and friction characteristics of the pure refrigerant HFC-134a during evaporation inside a vertical corrugated tube. The effects of heat flux, mass flux and evaporation temperature on the heat transfer coefficient and two-phase friction factor were also discussed. It is found that the percentage increases of the heat transfer coefficient and the two-phase friction factor of the corrugated tubes compared with those of the smooth tube were approximately 0–10 and 70–140 %, respectively. Balcilar et al. [19] investigated the best artificial intelligence method

to estimate the measured convective heat transfer coefficient and pressure drop of R134a flowing downward inside a vertical smooth copper tube using several ANN methods, such as multi layer perceptron (MLP), radial basis networks (RBFN), generalised regression neural network (GRNN) and adaptive neuro-fuzzy inference system (ANFIS). Colorado et al. [20] developed a physical–empirical model to investigate heat transfer of helical coil in oil and glycerol/water solution. They benefited from an artificial neural network (ANN) model working with equations of continuity, momentum and energy in each flow to have a reliable the natural convection heat transfer correlations. As a result of their analyses, it was found that saving time and improving general system performance were achieved using ANN.

Despite worthwhile experimental studies in the literature, relatively little information is currently available on numerical work such as ANN analysis on the evaporation heat transfer and flow characteristics in smooth and corrugated tubes. As mentioned previously, it is evident that the corrugated tubes have greater heat transfer potential than smooth tubes. As a consequence, in the present study the main concern is to fill this gap in the literature. The results for the solution of neural network analysis on the evaporation two-phase heat transfer coefficient and pressure drop, which have never before appeared in open literature, are presented. The large amount of measured data obtained from the experimental study regarding the convective heat transfer coefficient and pressure drop are compared with the results from ANN methods such as MLP and RBFN. In addition to this, the effect of input parameters (mass flux, heat flux, the temperature difference between the tube wall and saturation temperature, average vapour quality, evaporating temperature, two-phase friction factor, two-phase multiplier, liquid and vapour Reynolds numbers, Bond number, Froude number, Weber number, depth of corrugation and helix angle for the tested corrugated tubes) on the output parameters (convective heat transfer coefficient (h), pressure drop (ΔP)) is shown and discussed as a primary study on this subject in the literature. Moreover, correlation development study is performed to calculate the evaporation heat transfer coefficient using the most effective input parameters and the measured pressure drop values.

2 Experimental Apparatus and Method

A schematic diagram of the test apparatus is shown in Fig. 1. The refrigerant loop consists of a pre-heating loop, test sec-

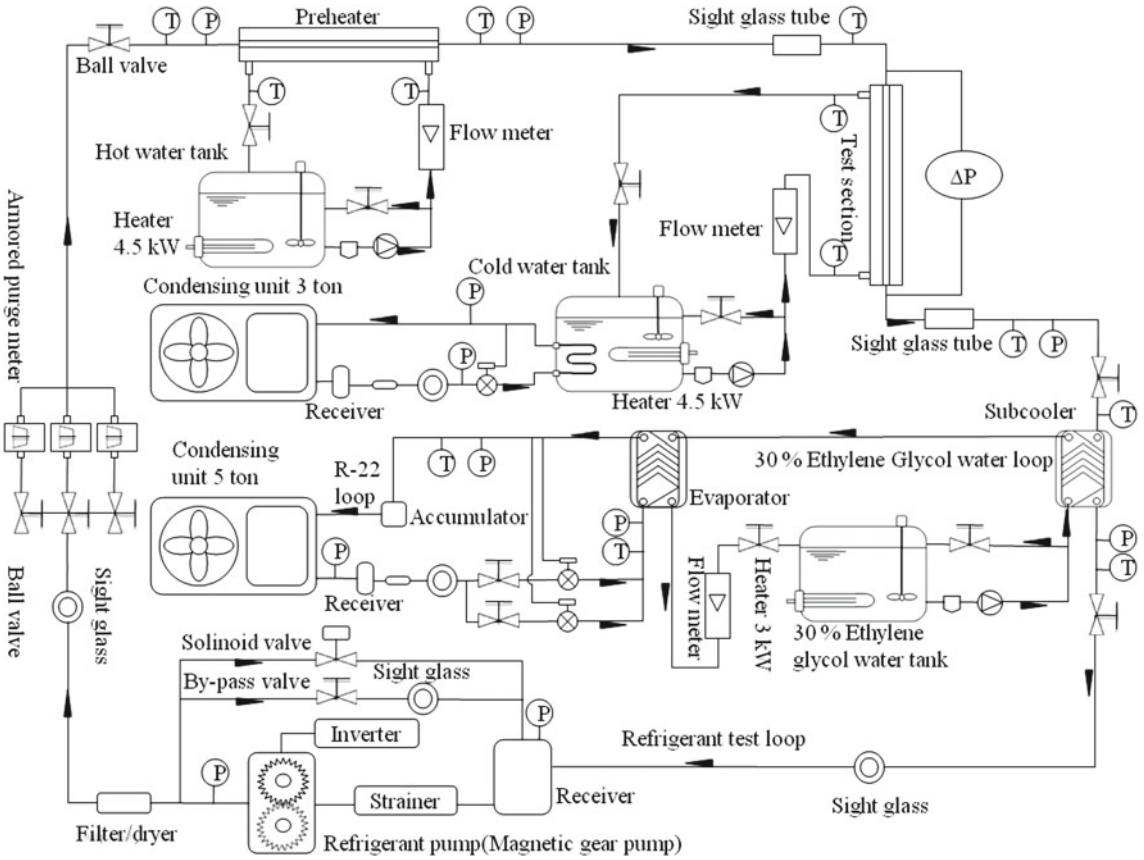

Fig. 1 Schematic diagram of experimental apparatus (from Aroonrat and Wongwises [18], with permission from Elsevier)

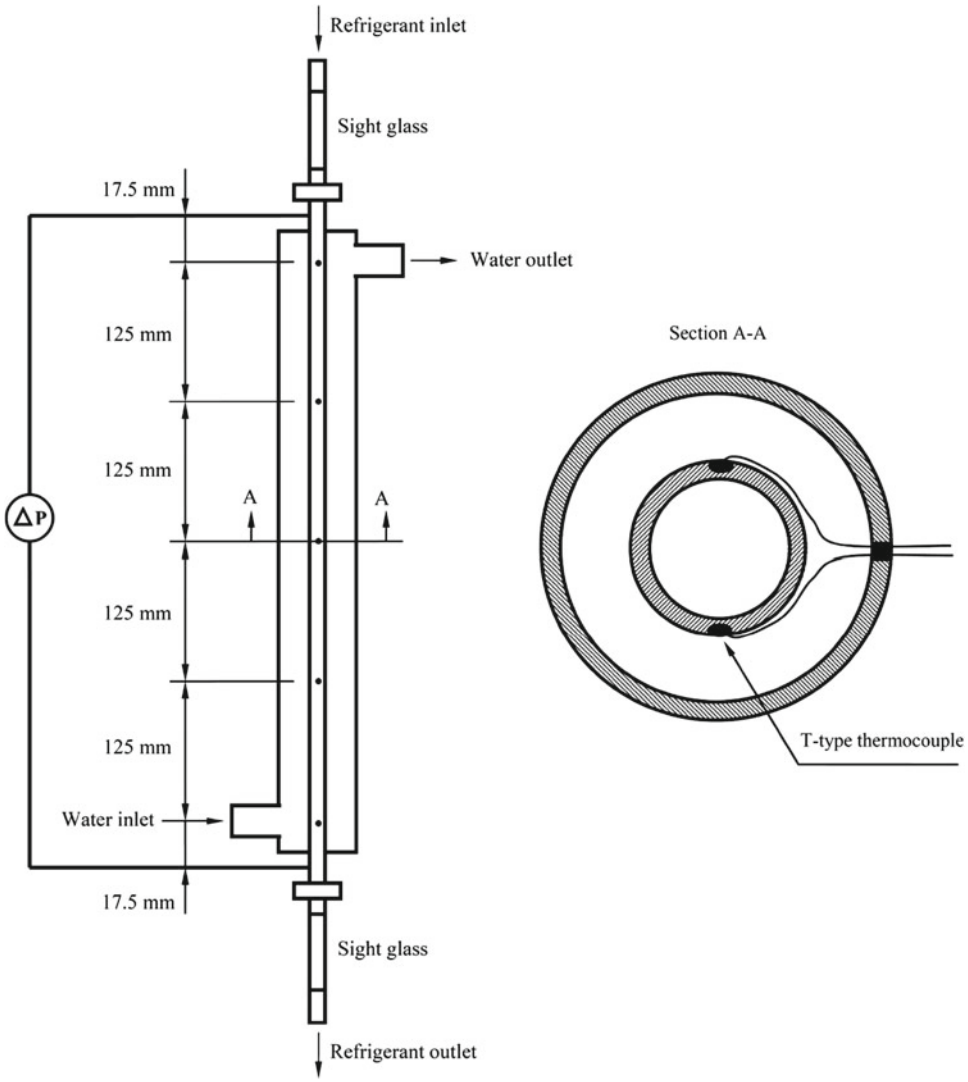

Fig. 2 Schematic diagram of the test section (from Aroonrat and Wongwises [18], with permission from Elsevier)

tion, heating loop and chilling loop. For the refrigerant circulating loop, liquid refrigerant is forced by a gear pump which can be adjusted to the flow rate using an inverter. The refrigerant then passes in series through a filter/dryer, a refrigerant flow meter, a pre-heater, and a sight glass and enters the test section. The pre-heater controls the inlet quality before entering the test section. It consists of a spiral counter-flow tube-in-tube heat exchanger which is designed to supply heat to prepare an inlet quality for the vaporization of the refrigerant. Leaving the test section, the refrigerant vapour then condenses inside a sub-cooler and is collected in a receiver. After leaving the chilling loop, the refrigerant returns from a two-phase refrigerant to a sub-cooled state. Eventually, the refrigerant returns to the refrigerant pump to complete the cycle.

Details of the test section are shown schematically in Fig. 2. The test section is a vertical counter-flow double tube heat exchanger with refrigerant flowing downward in the inner tube and heating water flowing upward in the annulus. The test sections are one smooth tube and five corrugated tubes, which are made from copper. The inner diameter and outer diameter of the inner tube are 8.7 and 9.52 mm, respectively. The length of the test section is 500 mm. Figure 3 shows a sketch and a photograph of a corrugated tube. The dimensions of the test section and the range of experimental conditions tested are listed in Tables 1 and 2, respectively. T-type thermocouples are installed at the inlet and outlet of the test section to measure the saturation temperature of the refrigerant. Similarly, the differential pressure transducer is installed to measure the pressure drop across the test section. The length between the pressure taps is 850 mm. There are 10 thermocouples located at five positions along the test section. All of the wall thermocouples are fixed with special glue having low thermal conductivity. The test section is insulated with rubber foam with a thermal conductivity of 0.04 W/mK. All of the thermocouples are well calibrated by standard thermometers with a precision of 0.1 °C. The refrigerant flow meter is a variable area type

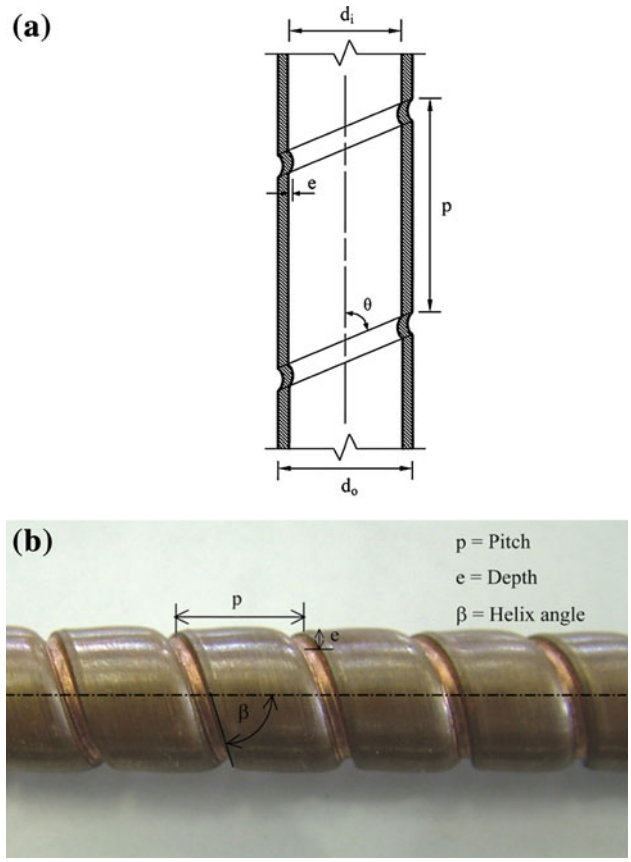

Fig. 3 Sketch (**a**) and photograph (**b**) of helically corrugated tube (from Aroonrat and Wongwises [18], with permission from Elsevier)

and is specially calibrated in the range of 0.2–3.4 LPM for R-134a by the manufacturer, as is the differential pressure transducer.

In the experiments, the inlet quality of the test section is varied by small increments. The imposed heat flux, mass flux and saturation temperature are kept constantly at the desired values. The system is allowed to approach a steady state before any data are recorded. During experiments, the temperature and pressure are continuously recorded along the test section by the data acquisition system. The uncertainties of measured quantities and calculated parameters, which are calculated from the root mean sum square method, are shown in Table 3.

3 Data Reduction and Experimental Uncertainty

The data reduction of the measured results can be analysed as follows:

3.1 The Inlet Vapour Quality of the Test Section ($X_{TS,in}$)

$$X_{\mathrm{TS,in}} = \frac{i_{\mathrm{TS,in}} - i_{\mathrm{l@T_{TS,in}}}}{i_{\mathrm{fg@T_{TS,in}}}}, \tag{1}$$

where $i_{\mathrm{l@T_{TS,in}}}$ is the enthalpy of the saturated liquid based on the temperature of the test section inlet, $i_{\mathrm{fg@T_{TS,in}}}$ is the enthalpy of vaporisation based on the temperature of the test section inlet, $i_{\mathrm{TS,in}}$ is the refrigerant enthalpy at the test section inlet and is given by

$$i_{\mathrm{TS,in}} = i_{\mathrm{ph,in}} + \frac{Q_{\mathrm{ph}}}{m_{\mathrm{ref}}}, \tag{2}$$

where $i_{\mathrm{ph,in}}$ is the inlet enthalpy of the liquid refrigerant before entering the pre-heater, m_{ref} is the mass flow rate of the refrigerant and Q_{ph} is the heat transfer rate in the pre-heater:

$$Q_{\mathrm{ph}} = m_{w,\mathrm{ph}} c_{p,w} (T_{w,\mathrm{in}} - T_{w,o})_{\mathrm{ph}}, \tag{3}$$

where $m_{w,\mathrm{ph}}$ is the mass flow rate of the water entering the preheater, $c_{p,w}$ is the specific heat of water and $(T_{w,\mathrm{in}} - T_{w,o})_{\mathrm{ph}}$ is the temperature difference between inlet and outlet positions of the preheater.

3.2 The Outlet Vapour Quality of the Test Section ($X_{TS,o}$)

$$X_{\mathrm{TS},o} = \frac{i_{\mathrm{TS},o} - i_{\mathrm{l@T_{TS,o}}}}{i_{\mathrm{fg@T_{TS,o}}}}, \tag{4}$$

where $i_{\mathrm{TS},o}$ is the refrigerant enthalpy at the test section outlet, $i_{\mathrm{l@T_{TS,o}}}$ is the enthalpy of the saturated liquid based on

Table 1 The dimensions of the test sections

Parameters	Smooth tube	Corrugated tube (A)	Corrugated tube (B)	Corrugated tube (C)	Corrugated tube (D)	Corrugated tube (E)
Outer diameter (mm)	9.52	9.52	9.52	9.52	9.52	9.52
Inner diameter (mm)	8.7	8.7	8.7	8.7	8.7	8.7
Length of test section (mm)	500	500	500	500	500	500
Inside tube area (mm^2)	13,665.9	14,514	14,938.1	15,362.1	15,951.4	16,582.8
Pitch of corrugation (mm)	–	12.7	12.7	12.7	8.46	6.35
Depth of corrugation (mm)	–	0.5	0.75	1	1	1
Helix angle (°)	–	53.875	53.875	53.875	64.07	69.95

Table 2 Experimental conditions

Controlled variable	Range
Refrigerant	R134a
Test tube material	Copper
Evaporating pressure, P_{sat}(bar)	4.14, 4.88, 5.71
Evaporating temperature, T_{sat} (°C)	10, 15, 20
Mass flux, G (kg m^{-2} s^{-1})	200, 300, 400
Heat flux, q (kW m^{-2})	19.91–30.64
Temperature difference, $\Delta T = T_{wi} - T_{sat}$, K	4.27–8.01
Average vapor quality, x	0.14–0.86

Table 3 Uncertainties of measured quantities and calculated parameters

Parameter	Uncertainty
Temperature, (T °C)	±0.1
Pressure drop, ΔP (kPa)	±0.37
Mass flow rate of refrigerant, m_{ref} (%)	±2 Full scale
Heat transfer rate of test section, Q_{TS} (%)	±15.01
Heat transfer rate of pre-heater, Q_{ph} (%)	±10.04
Average heat transfer coefficient, h_{exp} (%)	±15.01
Two-phase friction factor, f_{tp} (%)	±13.52
Average quality, x (%)	±7.63
Equivalent Reynolds number, Re_{eq} (%)	±6.03

the temperature of the test section outlet, and $i_{fg@T_{TS,o}}$ is the enthalpy of vaporisation. The outlet enthalpy of the refrigerant flow is calculated as follows:

$$i_{TS,o} = i_{TS,in} + \frac{Q_{TS}}{m_{ref}}, \tag{5}$$

where the heat transfer rate, Q_{TS}, in the test section is obtained from

$$Q_{TS} = m_{w,TS} c_{p,w} (T_{w,in} - T_{w,o})_{TS}, \tag{6}$$

where $m_{w,TS}$ is the mass flow rate of the water entering the test section, and $(T_{w,in} - T_{w,o})_{TS}$ is temperature difference between the outlet and inlet position of the test section.

3.3 The Average Heat Transfer Coefficient

$$h_{exp} = \frac{Q_{TS}}{A_{wi}(T_{wi} - T_{ref,sat})} \tag{7}$$

where h_{exp} is the experimental average heat transfer coefficient, Q_{TS} is the heat transfer rate in the test section, T_{wi} is the average temperature of the inner wall, $T_{ref,sat}$ is the average temperature of the refrigerant at the test section inlet and outlet, and A_{wi} is the inside surface area of the test section:

$$A_{wi} = \pi d L \tag{8}$$

where d is the inside diameter of the test tube, and L is the length of the test tube.

3.4 Calculation Procedure for the Generalised Artificial Neural Networks (ANNs) Model

An ANN is an information-processing system that has certain performance characteristics in common with biological neural networks. ANNs have been developed as generalisations of mathematical models of human cognition or neural biology, based on the assumptions that (1) information processing occurs at many simple elements called neurons, (2) signals are passed between neurons over connection links, (3) each connection link has an associated weight, which, in a typical neural net multiplies the signal transmitted, and (4) each neuron applies an activation function (usually non-linear) to its net input (sum of weighted input signals) to determine its output signal [21].

ANNs are such factors that can utilize machine learning for the duty of considered necessary mapping of the inputs to the outputs. A dataset is divided into three parts such as training, testing and validation. ANNs determine a function between the inputs and outputs generalizing the training group. The success of this group is calculated using the test group. The training duration of ANNs is determined by the validation group. When the training group has over fitting as a result of long time training, ANNs memorize the training group and its success on the test group reduces. The optimum point for the stop of training is determined using validation group.

As the ANNs are one of the most commonly used and developed models to investigate the relationship between linear or non-linear input–output patterns, they try to generalise the training group and then estimate the test group. Performance of ANNs is measured by the success of the prediction. There are many described ANN types and their architectures (different size of layers, neuron numbers and spread coefficients) related to function approximation in the literature. The most known methods are multi layer perceptron (MLP), radial basis functions networks (RBFN), generalised regression neural networks (GRNN) and artificial neural fuzzy inference system (ANFIS) which is the combination of fuzzy logic decision systems and ANNs. Schematic diagrams of artificial intelligence models used in the analysis, obtained by Matlab software [22], are shown in Fig. 4.

3.4.1 Multi Layer Perceptron (MLP)

An artificial neuron performs the duty of taking weighted total of the inputs and evaluates it by an activation function. The single-layer perceptron is used for the linear problems and cannot be applied for the non-linear in nature. All perceptrons of MLP are arranged in an orderly manner of layers.

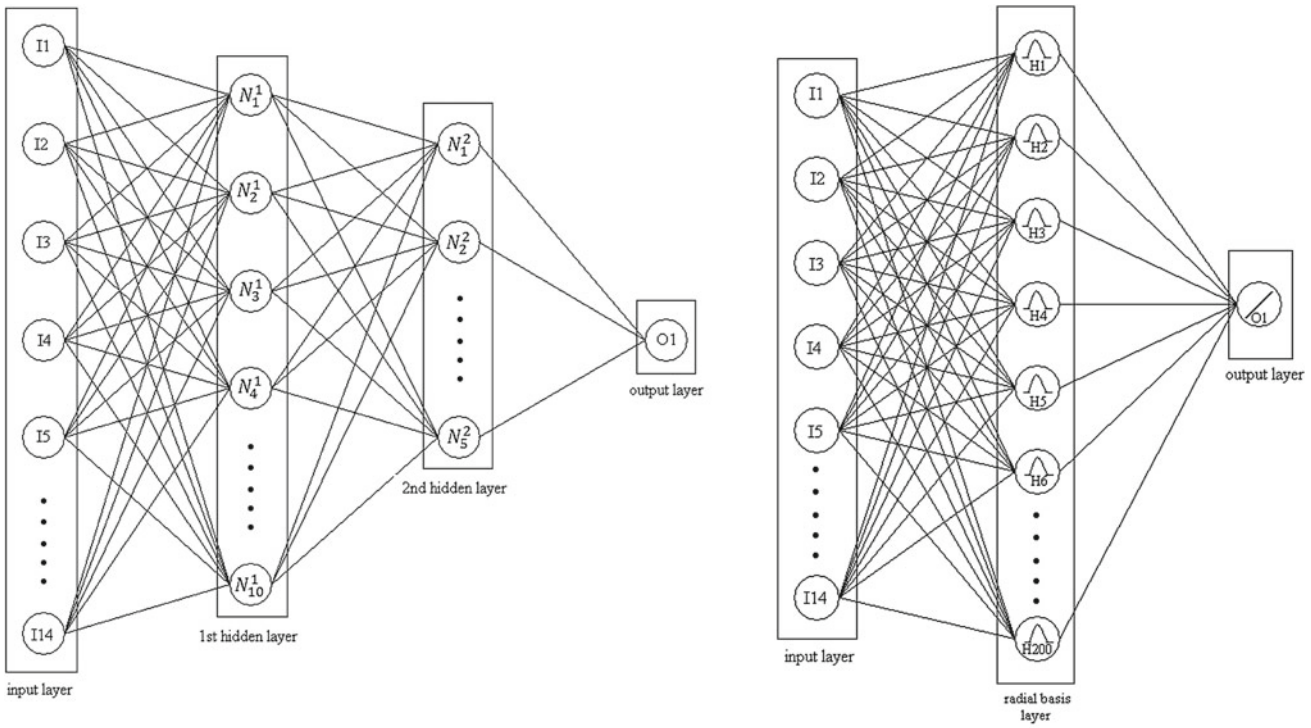

(a) Multi layer perceptron (MLP) with 10-5-1 architecture

(b) Artificial neural fuzzy inference system (ANFIS)

Fig. 4 Schematic diagrams of artificial intelligence models used in the analysis

The initial layer is the input layer and is called as passive layer. It should be noted that the inputs are passed to the next layer for processing after the first one. The output layer forms the last layer and is called as the active layer. These neurons take the inputs in the structure of neural connections among the neurons. Each connection has a weight connected with it. The computation of the weighted average of the input and its application to the activation function are performed by each neuron.

MLP is the member of the feed-forward network family. According to this method, the number of input and output neurons is equal to the number of input and output parameters, and there are some layers including neurons between them. Specification of non-linearity and calculation process increases with increasing numbers of hidden layers and neurons. Different architectures of MLP were used for the calculation of heat transfer coefficient and pressure drop. All neurons of MLP are connected with another neurons in the next layer making massive number of connections between the various connections and the direction of these connections are forward which means that the way of the connection among neurons is not recurrent. A Levenberg–Marquardt algorithm, based on the method of back propagation, was used for the training process to model the outputs using inputs of the problem.

3.4.2 Radial Basis Function Networks (RBFN)

This model has a simple 3-layer ANN architecture: input layer, hidden layer and output layer.

RBFN architecture has a single hidden layer and some similarities with the MLP method. On the other hand, it has a different calculation process for the determination of the neuron number, different activation function including Gaussian or exponential manner and difference in neuron number in the hidden layer. RBFN's single-layer architecture has equal neuron numbers with the element numbers in the training group. Bias numbers are the control parameters of RBFN architecture and should be determined by the user as trial and error method during calculations in Matlab Software [22]. Training of this architecture, in other words, values of neuron connections, are calculated using training group by means of least square method [22] as its training algorithm.

3.5 Correlation Development

Determination of heat transfer characteristics of compact systems such as heat transfer coefficient, frictional pressure drop, flow type between the fluids and heat transfer surface area in heat exchangers should be determined accurately for the optimum design. The two-phase heat trans-

fer systems have a higher thermal heat transfer performance than single-phase heat transfer systems in limited apparatus volumes. The advantage of high thermal performance in comparison with the single-phase applications includes smaller, more compact systems regarding tube length, tube diameter and internal tube geometry shape in a wide variety of applications, e.g. refrigeration and air conditioning systems, power engineering and other thermal processing plants. Before doing any numerical work on this subject, the validation process of the experimental setup and data is very significant with regard to the reliability of the study. The correctness of experimental data should be evaluated by either graphics regarding the characteristics of trend lines such as alteration of heat transfer coefficient versus quality, heat flux versus temperature difference between the vapour and inlet wall temperature, pressure drop versus vapour quality etc., or by widely accepted correlations in the literature, and desired working conditions should be agreeable with the heat balance correlations and flow type observations by means of sight glasses at the different points of the experimental apparatus.

There have been a number of studies on the in-tube evaporation heat transfer coefficient and pressure drop. The frictional, acceleration and gravitational components determine the two-phase total pressure drop in tubes. Determination of the void fraction is required to compute the acceleration and gravitational components, and in a similar way the determination of either the two-phase friction factor or the two-phase frictional multiplier is required to compute the frictional component of the pressure drop. Generally, empirical methods have been used to compute the evaporation heat transfer coefficients and pressure drops in tubes.

The correlation for the laminar and turbulent flow inside the test tube was developed as a form of Dittus and Boelter's [23] correlation in Eq. (9) by means of several dimensionless numbers which were defined in the following section. As a result, Eq. (9) is formed to predict the convective condensation heat transfer coefficient in terms of the above explanations as follows:

$$h = A\left(\frac{k_l}{d}\right)(\mathrm{Re}_g)^B (f_{\mathrm{tp}})^C (\mathrm{Fr})^D (x)^E (\mathrm{Bo})^F (\Delta \mathrm{T}_{\mathrm{sat}})^G (\phi_l^2)^H \times (\mathrm{We})^I \left(\Delta P \frac{L}{P}\right)^J (\mathrm{Re}_l)^K \tag{9}$$

3.6 Definition of Input Parameters of the Artificial Neural Network (ANN) Analysis

The total pressure gradient is the sum of three contributions: the gravitational pressure gradient, the momentum pressure gradient and the frictional pressure gradient as follows:

Table 4 Elimination of ANN methods belonging to all the tested tubes according to the error rates for pressure drop (a) and convective heat transfer coefficients (b) for the mass fluxes of 200, 300, 400 kg m^{-2} s^{-1} and $T_{sat} = 10$, 15 and 20 °C.

ΔP L^{-1} (kPa m^{-1})	Error analysis /ANN methods		Square law
	R square	Proportional (%)	
(a)			
MLP 10-5-1	0.999993	0.001677	0.043752
MLP 10-1	0.999988	0.012214	0.754229
MLP 5-1	0.999991	0.006793	0.22766
MLP 2-1	0.998872	0.054519	10.9036
RBF 1,000	0.029942	5.06416	66761.6
RBF 10,000	0.723309	3.712494	35227.66
RBF 100,000	0.980169	0.370425	502.1212
RBF 1,000,000	0.976075	0.462784	647.2979
RBF 1,000,000	0.905844	2.537781	14,664
(b)			
MLP 10-5-1	0.9999996	0.358	0.000198
MLP 10-1	0.999993	0.438	0.000316
MLP 5-1	0.999998	0.561	0.000259
MLP 2-1	0.999905	5.685	0.030739
RBF 1,000	0.447754	682.017	1,927.148
RBF 10,000	0.731676	59.682	8.71043
RBF 100,000	0.995606	18.519	0.538876
RBF 1,000,000	0.994327	22.937	0.649612
RBF 1,000,000	0.871393	98.393	2.556523

$$\frac{d\mathrm{P}}{d\mathrm{z}} = \left(\frac{d\mathrm{P}}{d\mathrm{z}}\right)_G + \left(\frac{d\mathrm{P}}{d\mathrm{z}}\right)_M + \left(\frac{d\mathrm{P}}{d\mathrm{z}}\right)_F \tag{10}$$

Pressure drop due to gravity can be determined from

$$(\Delta P)_G = -g\left(\alpha\rho_g + (1-\alpha)\rho_l\right) L \tag{11}$$

where the void fraction, a, can be determined from the Zivi correlation [24] stated below:

$$\alpha = \frac{1}{1 + \left(\frac{1-x}{x}\right)\left(\frac{\rho_g}{\rho_l}\right) S} \tag{12}$$

$$S = \left(1 - x + x\frac{\rho_l}{\rho_g}\right)^{1/2} \tag{13}$$

The momentum pressure gradient can be defined as follows:

$$\left(\frac{d\mathrm{P}}{d\mathrm{z}}\right)_M = -G^2 \frac{d}{d\mathrm{z}}\left[\frac{x^2}{\rho_g \alpha} + \frac{(1-x)^2}{\rho_l(1-\alpha)}\right] \tag{14}$$

The two-phase frictional pressure gradient can be obtained by subtracting the gravitational and momentum terms from the total measured pressure drop as follows:

Table 5 The most predictive input parameters according to the error rates for all tested tubes

Inputs														Input number	Outputs	
I	II	III	IV	V	VI	VII	VIII	IX	X	XI	XII	XIII	XIV		R^2–ΔP (%)	R^2–h (%)
0	0	0	0	0	0	0	0	0	0	0	0	1	0	1	0.614656	0.619369
0	0	0	0	0	0	0	0	0	1	0	0	0	0	1	0.606841	0.643204
0	0	0	0	0	0	0	0	0	0	0	1	0	0	1	0.561001	0.556516
1	0	0	0	0	0	0	0	0	0	0	0	0	0	1	0.271441	0.289444
0	0	0	0	1	0	0	0	0	0	0	0	0	0	1	0.219961	0.128164
0	0	0	0	0	1	0	0	0	0	0	0	0	0	1	0.215296	0.134689
0	1	0	0	0	0	0	0	0	0	0	0	0	0	1	0.178929	0.209764
0	0	0	0	0	0	0	0	0	0	1	0	0	0	1	0.124609	0.145161
0	0	1	0	0	0	0	0	0	0	0	0	0	0	1	0.080089	0.191844
0	0	0	1	0	0	0	0	0	0	0	0	0	0	1	0.038416	0.148225
0	0	0	0	0	0	1	0	0	0	0	0	0	0	1	0.000289	0.008649
0	0	0	0	0	0	0	0	1	0	0	0	0	0	1	0.0036	0.000961
0	0	0	0	0	0	0	0	0	0	0	0	0	1	1	0.088209	0.020736
0	0	0	0	0	0	0	1	0	0	0	0	0	0	1	0.093636	0.053824

Table 6 The most predictive combinations of input parameters according to the error rates for the two known input parameters

Inputs														Input number	Outputs	
I	II	III	IV	V	VI	VII	VIII	IX	X	XI	XII	XIII	XIV		R^2–ΔP (%)	R^2–h (%)
0	0	0	0	0	0	1	0	0	1	0	0	0	0	2	0.970225	0.863041
0	0	0	0	0	0	1	0	0	0	0	1	0	1	2	0.929296	0.748225
0	0	0	0	0	1	0	0	0	0	0	0	1	0	2	0.915849	0.8836
0	0	0	0	1	0	0	0	0	0	0	0	1	0	2	0.913936	0.799236
0	0	0	0	0	1	0	0	0	1	0	0	0	0	2	0.893025	0.876096
0	0	0	0	1	0	0	0	0	1	0	0	0	0	2	0.891136	0.776161
0	0	0	1	0	0	0	0	0	0	0	0	0	1	2	0.874225	0.9999
0	0	0	0	0	1	0	0	0	0	0	1	0	0	2	0.872356	0.801025
0	0	0	0	0	0	1	0	0	0	0	0	1	0	2	0.870489	0.802816
0	0	0	0	0	0	0	1	0	0	0	0	0	1	2	0.848241	0.986049
0	0	0	0	1	0	0	0	0	0	0	1	0	0	2	0.8464	0.710649
0	0	0	0	0	0	0	0	0	1	0	0	0	1	2	0.817216	0.933156
0	0	0	0	0	0	0	0	0	0	0	0	1	1	2	0.762129	0.948676
0	0	0	0	0	0	0	0	0	0	0	1	0	1	2	0.677329	0.877969
1	0	0	0	0	0	0	0	0	0	0	0	0	1	2	0.6724	0.7744
0	0	0	0	0	0	0	0	0	0	1	0	0	1	2	0.627264	0.727609
0	0	0	0	0	0	0	0	1	0	0	0	1	0	2	0.616225	0.664225
0	0	0	0	0	1	1	0	0	0	0	0	0	0	2	0.611524	0.64

$$\left(\frac{d\mathrm{P}}{d\mathrm{z}}\right)_F = \left(\frac{d\mathrm{P}}{d\mathrm{z}}\right)_{\mathrm{Exp}} - \left(\frac{d\mathrm{P}}{d\mathrm{z}}\right)_G - \left(\frac{d\mathrm{P}}{d\mathrm{z}}\right)_M \tag{15}$$

The two-phase friction factor is calculated by the following equation based on the equivalent Reynolds number:

$$f_{\mathrm{tp}} = \left(\frac{d\mathrm{P}}{d\mathrm{z}}\right)\frac{\rho_l d^3}{2\mathrm{Re}_{\mathrm{eq}}^2 \mu_l^2}, \tag{16}$$

where the all liquid equivalent Re number is determined from

$$\mathrm{Re}_{\mathrm{eq}} = \frac{G_{\mathrm{eq}} d}{\mu_l} \tag{17}$$

and the equivalent liquid mass flux is defined as

$$G_{\mathrm{eq}} = G\left((1-x) + x\left(\frac{\rho_l}{\rho_g}\right)^{0,5}\right) \tag{18}$$

Table 7 The most predictive combinations of input parameters according to the error rates for the three known input parameters

Inputs														Input number	Outputs	
I	II	III	IV	V	VI	VII	VIII	IX	X	XI	XII	XIII	XIV		R^2–ΔP (%)	R^2–h (%)
0	0	0	0	0	0	1	0	1	0	0	0	1	0	3	0.998001	0.933156
0	1	0	0	0	0	1	0	0	0	0	0	1	0	3	0.998001	0.923521
0	0	0	0	0	0	1	0	0	1	0	0	1	0	3	0.998001	0.906304
1	0	0	0	0	0	1	0	0	0	0	0	1	0	3	0.998001	0.942841
0	0	0	0	0	0	1	0	0	0	0	1	1	0	3	0.998001	0.893025
0	0	0	0	0	0	1	0	0	0	1	0	1	0	3	0.996004	0.925444
0	0	0	0	0	0	1	0	1	0	0	1	0	0	3	0.994009	0.933156
1	0	0	0	0	0	1	0	1	0	0	0	0	0	3	0.994009	0.900601
1	0	0	0	0	0	1	0	0	1	0	0	0	0	3	0.994009	0.948676
0	0	0	0	0	0	1	0	1	1	0	0	0	0	3	0.992016	0.944784
0	0	0	0	0	0	1	0	0	0	1	1	0	0	3	0.992016	0.819025
0	0	0	0	0	0	1	0	1	0	1	0	0	0	3	0.990025	0.946729
0	1	0	0	0	0	1	0	1	0	0	0	0	0	3	0.990025	0.9409
0	1	0	0	0	0	1	0	0	1	0	0	0	0	3	0.990025	0.925444
0	0	0	0	0	0	1	1	0	1	0	0	0	0	3	0.988036	0.8836
1	1	0	0	0	0	1	0	0	0	0	0	0	0	3	0.986049	0.929296
1	0	0	0	0	0	1	0	0	0	0	1	0	0	3	0.984064	0.829921
0	0	0	0	0	0	1	0	0	1	1	0	0	0	3	0.984064	0.887364
0	0	0	0	0	0	1	0	0	1	0	1	0	0	3	0.984064	0.887364
0	0	0	0	0	0	1	1	0	0	0	1	0	0	3	0.982081	0.904401
0	0	1	0	0	0	1	0	0	0	0	1	0	0	3	0.976144	0.887364
0	1	0	0	0	0	1	0	0	0	1	0	0	0	3	0.972196	0.946729
0	0	0	0	1	0	1	0	0	1	0	0	0	0	3	0.972196	0.891136
0	0	1	0	0	0	1	0	0	1	0	0	0	0	3	0.972196	0.877969
0	0	0	0	0	1	1	0	0	1	0	0	0	0	3	0.972196	0.906304
1	0	0	0	1	0	0	0	0	0	0	0	1	0	3	0.970225	0.885481
0	0	0	0	1	0	0	0	0	0	0	1	1	0	3	0.970225	0.8836
0	0	0	0	1	0	0	0	0	1	0	0	1	0	3	0.964324	0.885481
0	1	0	0	0	1	0	0	0	0	0	1	0	0	3	0.964324	0.948676
0	0	0	0	0	0	1	0	0	1	0	0	0	1	3	0.964324	0.9801
0	1	0	0	0	0	1	0	0	0	0	0	0	1	3	0.964324	0.908209
0	0	0	0	1	0	0	0	1	1	0	0	0	0	3	0.962361	0.908209
0	0	0	0	0	1	0	0	0	0	0	1	1	0	3	0.962361	0.952576
0	0	0	0	1	0	0	0	0	0	0	0	1	0	3	0.962361	0.6724
0	1	0	0	0	1	0	0	0	0	0	0	1	0	3	0.962361	0.962361
0	0	0	0	0	1	0	0	1	0	0	0	1	0	3	0.962361	0.950625
1	0	0	0	1	0	0	0	0	1	0	0	0	0	3	0.962361	0.906304
0	0	0	0	0	1	0	0	1	1	0	0	0	0	3	0.9604	0.9409
0	1	0	0	0	1	0	0	1	0	0	0	0	0	3	0.9604	0.956484
1	1	0	0	1	0	0	0	0	0	0	0	0	0	3	0.9604	0.923521
0	0	0	0	0	1	0	0	1	0	0	1	0	0	3	0.9604	0.956484
0	0	0	0	1	0	0	1	0	0	0	0	1	0	3	0.9604	0.906304
1	0	0	0	0	1	0	0	0	0	0	1	0	0	3	0.958441	0.861184
1	0	0	0	0	1	0	0	1	0	0	0	0	0	3	0.956484	0.935089
0	1	0	0	0	1	0	0	0	1	0	0	0	0	3	0.956484	0.844561
0	0	0	0	0	1	0	0	0	1	0	0	1	0	3	0.956484	0.950625

Table 7 continued

Inputs														Input number	Outputs	
I	II	III	IV	V	VI	VII	VIII	IX	X	XI	XII	XIII	XIV		R^2–ΔP (%)	R^2–h (%)
1	0	0	0	0	1	0	0	0	1	0	0	0	0	3	0.956484	0.948676
0	1	0	0	1	0	0	0	0	0	1	0	0	0	3	0.954529	0.912025
0	1	0	0	1	0	0	0	0	0	0	0	1	0	3	0.954529	0.906304
0	0	0	0	0	0	1	1	0	0	0	0	1	0	3	0.954529	0.887364
0	0	0	0	1	0	0	0	0	1	1	0	0	0	3	0.954529	0.896809
0	0	0	0	1	0	0	0	1	0	0	0	1	0	3	0.952576	0.906304
0	0	0	0	0	0	1	0	0	0	0	0	1	1	3	0.952576	0.982081

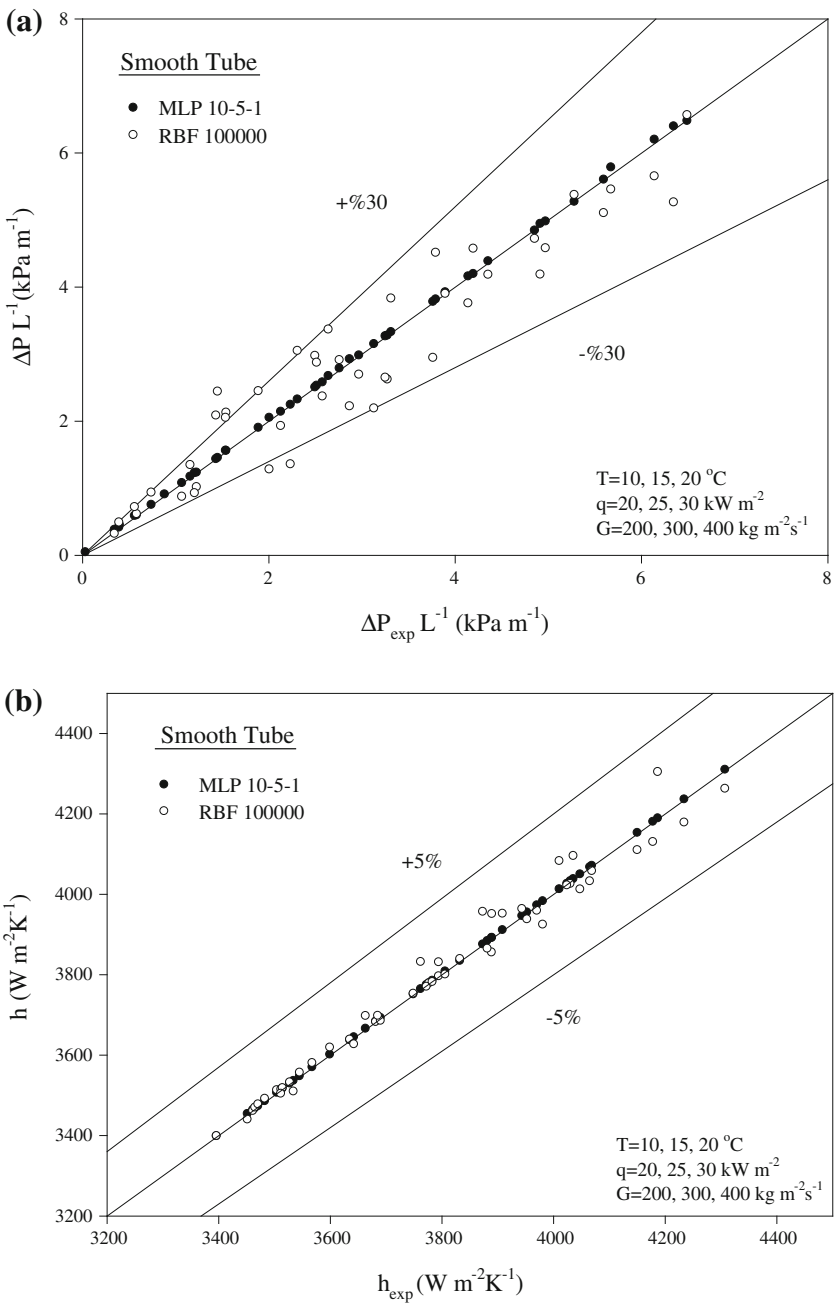

Fig. 5 Comparisons of experimental pressure drop (**a**) and convective heat transfer coefficients (**b**) with the artificial neural network methods for the smooth tube

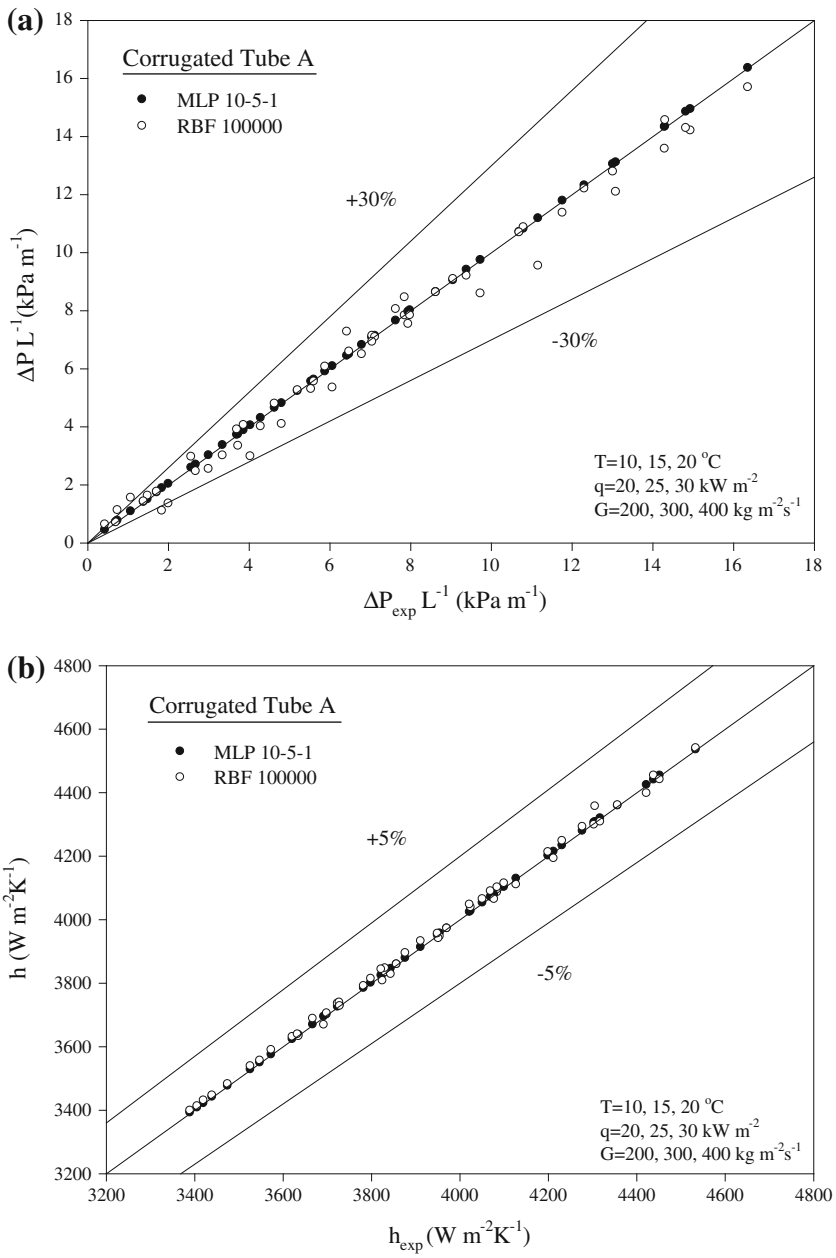

Fig. 6 Comparisons of experimental pressure drop (**a**) and convective heat transfer coefficients (**b**) with the artificial neural network methods for the corrugated tube A

Bond number (Bo), liquid and vapour Reynolds numbers ($\mathrm{Re_l}$, $\mathrm{Re_g}$), two-phase multiplier (ϕ_l^2), Froude number (Fr) and Weber number (We) are defined, respectively, as follows:

$$\mathrm{Bo} = \frac{q}{i_{\mathrm{fg}} G} \tag{19}$$

$$\mathrm{Re}_l = \frac{\mathrm{Gd}(1-x)}{\mu_l} \tag{20}$$

$$\mathrm{Re}_g = \frac{\mathrm{Gdx}}{\mu_g} \tag{21}$$

$$\phi_l^2 = 1 + \frac{C}{X} + \frac{1}{X^2} \tag{22}$$

where Martinelli parameter is defined as

$$X_{\mathrm{tt}} = \left(\frac{1-x}{x}\right)^{0.9} \left(\frac{\rho_g}{\rho_l}\right)^{0.5} \left(\frac{\mu_l}{\mu_g}\right)^{0.1} \tag{23}$$

The constant C in Eq. (22) is the parameter which indicates the two-phase flow condition. The value of this parameter, proposed by Chisholm [25] and varying from 5 to 20, depends on the flow condition of the vapour and liquid. For instance, the constant $C = 20$ when the vapour and liquid flow is in the turbulent region, and $C = 5$ if the two-phase flow is in the laminar region.

$$\mathrm{Fr} = \frac{G^2}{\mathrm{gd}\rho_{\mathrm{TP}}^2}, \tag{24}$$

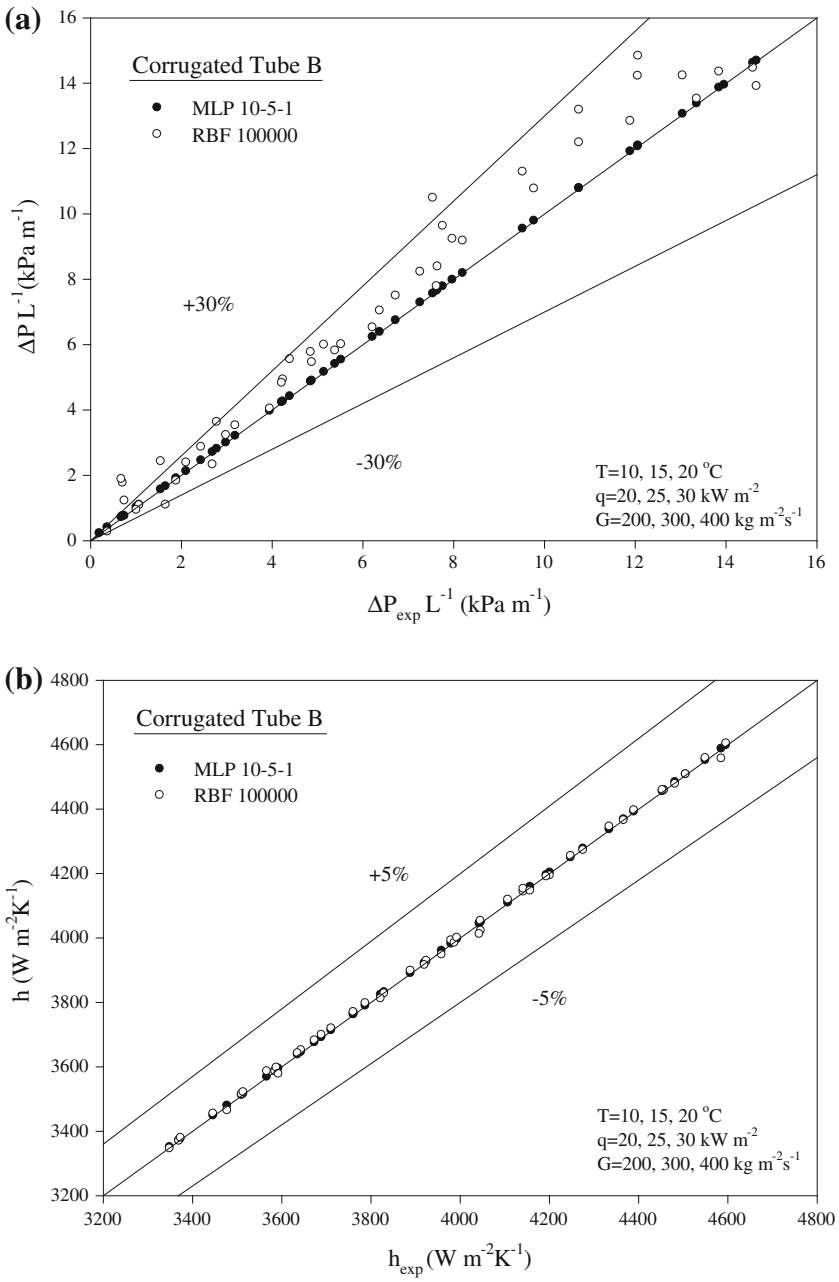

Fig. 7 Comparisons of experimental pressure drop (**a**) and convective heat transfer coefficients (**b**) with the artificial neural network methods for the corrugated tube B

where the two-phase density is determined from

$$\rho_{\mathrm{TP}} = \left(\frac{x}{\rho_g} + \frac{1-x}{\rho_l}\right)^{-1} \tag{25}$$

$$\mathrm{We} = \frac{G^{2\mathrm{d}}}{\rho_{\mathrm{TP}}\sigma} \tag{26}$$

Reynolds equivalent number, Lockhart and Martinelli parameter, Weber number, Bond and Froude numbers were used as the most significant variables in the proposed correlation. Reynolds number gives a measure of the ratio of inertial forces to viscous forces characterising different flow regimes such as laminar and turbulent flow. Lockhart and Martinelli parameter is used in internal two-phase flow calculations expressing the liquid fraction of a flowing fluid. Weber number is used for fluid flows where there is an interface between two different fluids, and it can be considered as a measure of the relative significance of the fluid's inertia compared with its surface tension. Bond number expresses the ratio of body forces to surface tension forces, low Bond numbers indicate the surface tension domination on the system and Froude number is used to compare inertial and gravitational forces. The effect of other important parameters belonging to the fluid properties such as liquid and vapour phases of

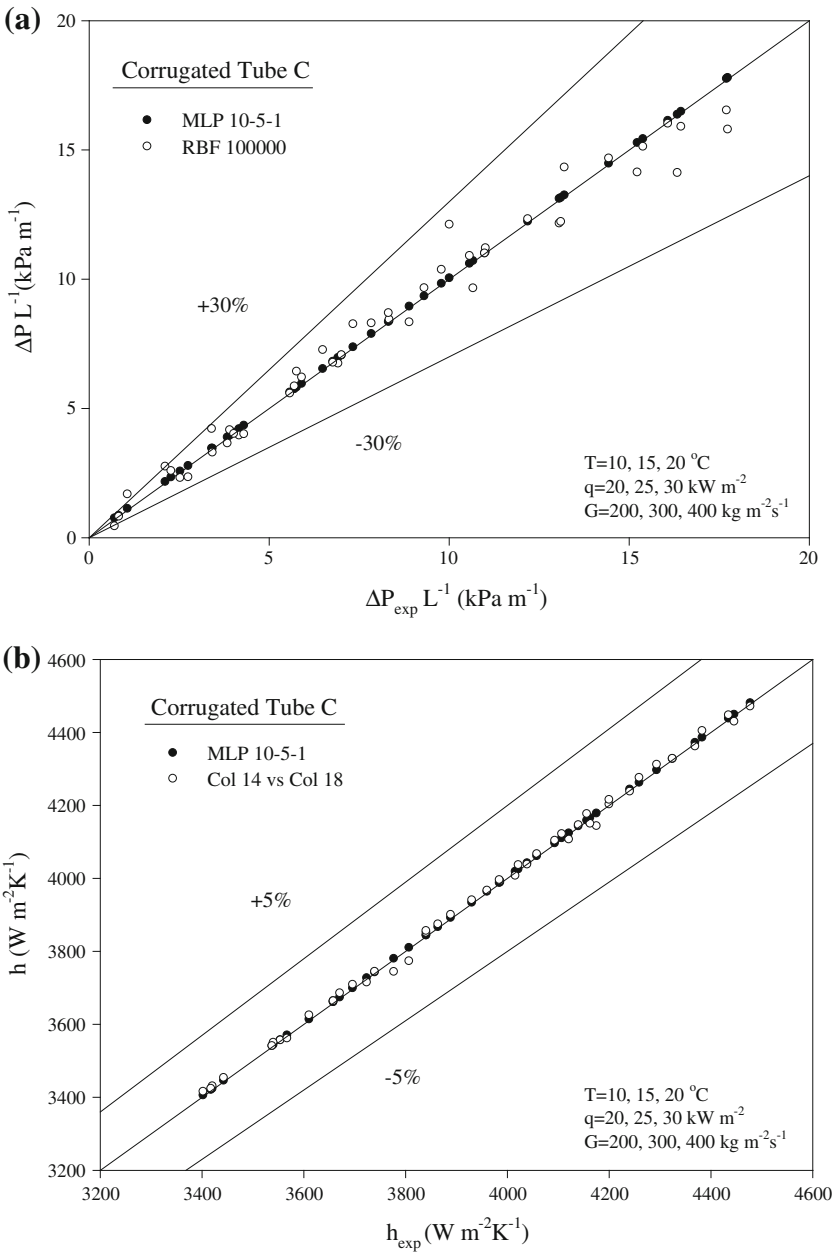

Fig. 8 Comparisons of experimental pressure drop (**a**) and convective heat transfer coefficients (**b**) with the artificial neural network methods for the corrugated tube C

density, dynamic viscosity, kinematic viscosity and thermal diffusivity exist in the Prandtl number and other dimensionless numbers.

3.7 Error Analysis

Error analysis of the study is performed by means of Eqs. (27), (28) and (29) and the results are given in Tables 4, 5, 6 and 7. In these equations, N is the element number of the test group, h^i_{exp} and h^i_{calc} are the experimental and calculated results of the heat transfer coefficient obtained from "i" number of test data, and $\overline{h}_{\text{exp}}$ and $\overline{h}_{\text{calc}}$ are the average values of experimental and calculated results of heat transfer coefficient obtained from the numerical analysis. It should be noted that error analysis of pressure drop was carried out similarly.

The R-square error is determined as follows:

$$E_{\text{Rsquare}} = \frac{\left(\sum_{i=1}^{N}(h^i_{\text{exp}} - \overline{h}_{\text{exp}})(h^i_{\text{calc}} - \overline{h}_{\text{calc}})\right)^2}{\left(\sum_{i=1}^{N}(h^i_{\text{exp}} - \overline{h}_{\text{exp}})^2\right)\left(\sum_{i=1}^{N}(h^i_{\text{calc}} - \overline{h}_{\text{calc}})^2\right)} \tag{27}$$

Proportional error is calculated as follows:

$$E_{\text{ratio}} = \frac{100}{N}\sum_{i=1}^{N}\frac{\left|h^i_{\text{exp}} - h^i_{\text{calc}}\right|}{h^i_{\text{exp}}} \tag{28}$$

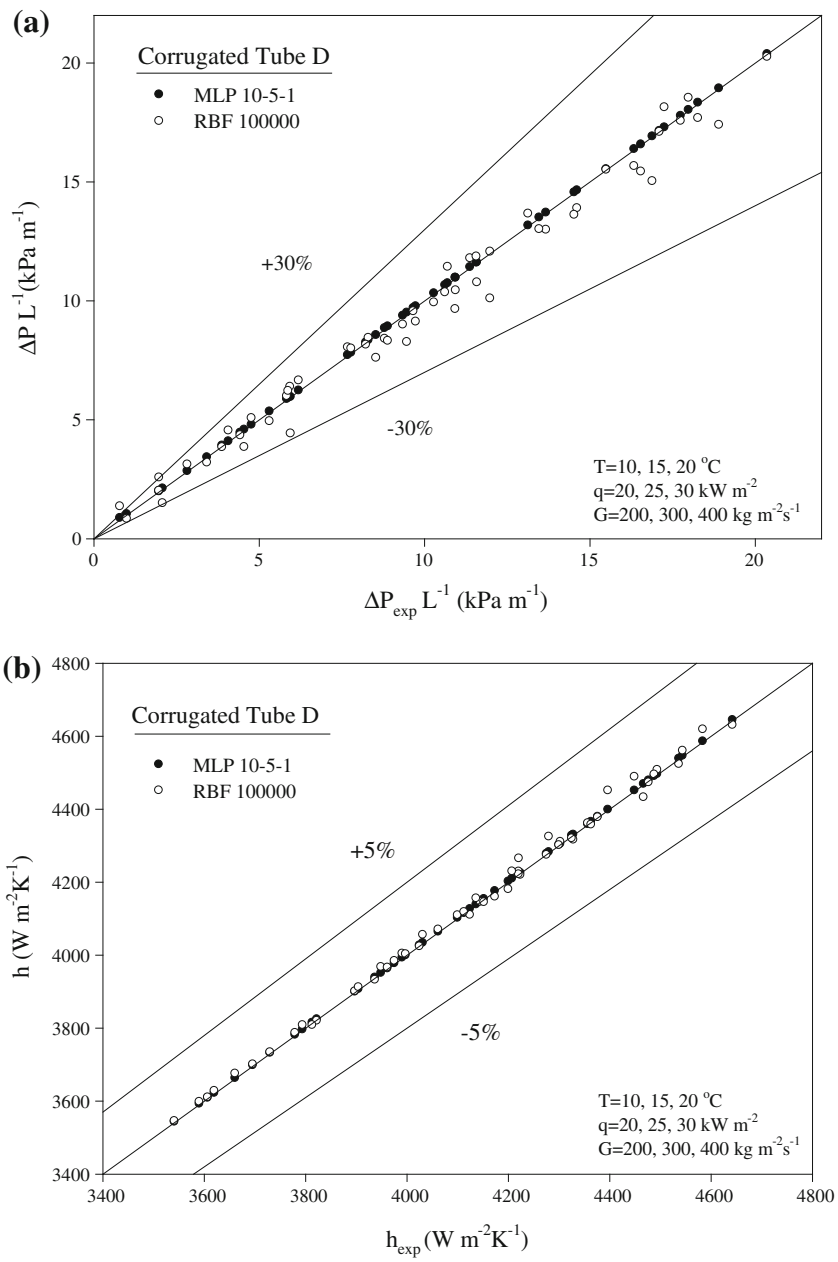

Fig. 9 Comparisons of experimental pressure drop (**a**) and convective heat transfer coefficients (**b**) with the artificial neural network methods for the corrugated tube D

Square law error is estimated as follows:

$$E_{\text{square}} = \sqrt{\frac{1}{N}.\sum_{i=1}^{N}(h^i_{\text{exp}} - h^i_{\text{calc}})^2} \tag{29}$$

4 Results and Discussion

The experiments of the present study were performed at the Fluid Mechanics, Thermal Engineering and Multiphase Flow Research Lab. (FUTURE) in KMUTT. Pure HFC-134a was used in the experiments. Special attention was paid to the accuracy of the measurements during the experiments as can be seen from authors' previous publications on in-tube evaporation processes.

Numerical analysis of artificial intelligence includes six-dimensional input parameters, such as mass flux (G, kg m^{-2} s^{-1}), heat flux (q, kW m^{-2}), saturation temperature (T_{sat}, °C), temperature difference between the tube wall and saturation temperature ($\Delta T_{\text{sat}} = T_{\text{wi}} - T_{\text{sat}}$), depth of corrugation (e, mm) and helix angle (β,°) for the tested corrugated tubes and eight-dimensionless input parameters, such as average vapour quality (x), two-phase friction factor (f_{tp}), two-phase multiplier (ϕ_l^2), liquid and vapour Reynolds numbers (Re_l, Re_g), Bond number (Bo), Froude number (Fr), Weber

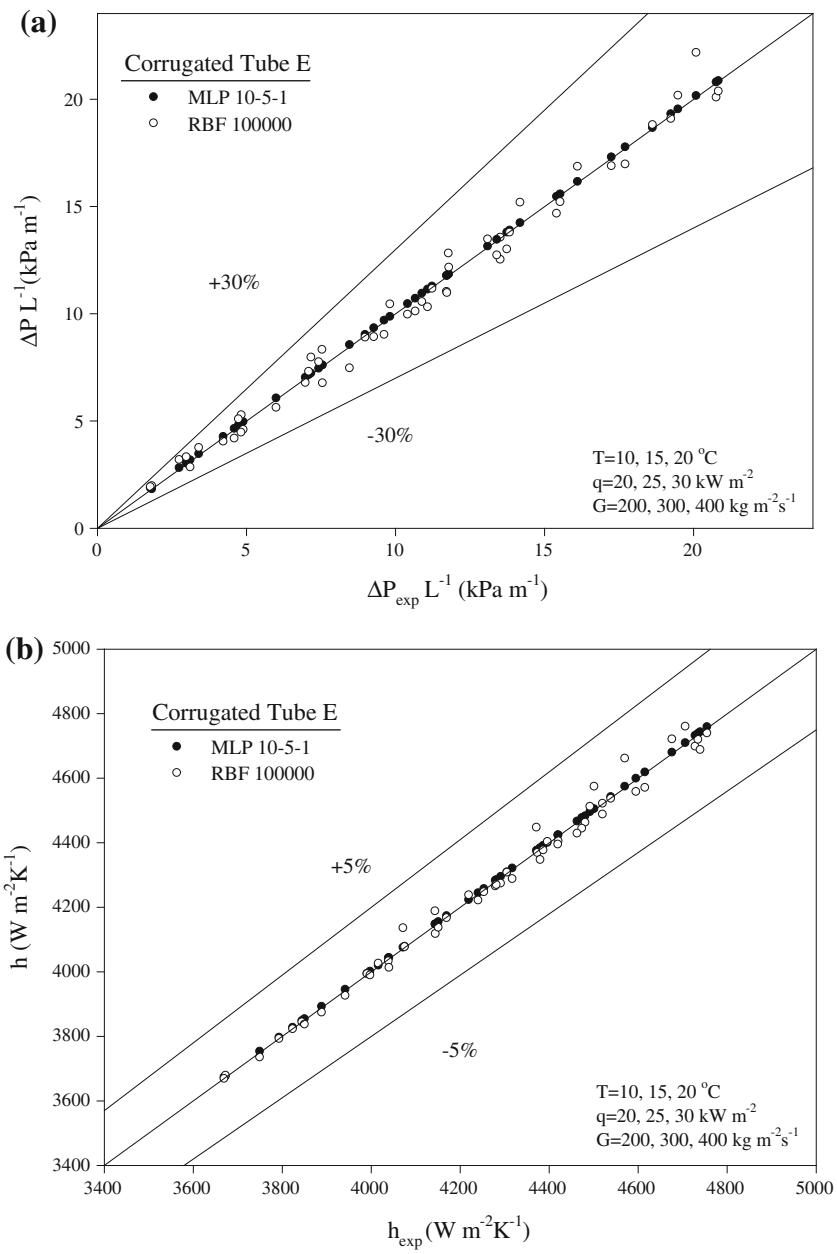

Fig. 10 Comparisons of experimental pressure drop (**a**) and convective heat transfer coefficients (**b**) with the artificial neural network methods for the corrugated tube E

number (We), two-dimensional output parameters such as convective heat transfer (h, W m^{-2} K^{-1}) and pressure drop (ΔP, Pa).

The K-fold cross validation algorithm is one of the best ways to measure the modelling success of the experimental data [26]. The coefficient of this algorithm (K) was chosen as 5. First, all data (300 data points) were divided into 5 equal sets according to this algorithm. Then, one of the 5 sets was assigned as test one, the other 4 sets became training one and the system was started to train. After that, the success rate was checked for the separated test set. At this stage, the systems' success had been measured for 1/5 data. This process was continued by changing the data sets which were used for test and training, and the success of the system was measured using the altered test set. As a result, the modelling performance of all data was measured at the end. There are several architectures tried in the analysis such as 10-5-1, 10-1 and 2-1. The random set for 20 % of the training sets was separated to prevent excess learning of the artificial intelligence during the application of the MLP algorithm. In this case, the sets of training, validation and test were determined with 192, 48 and 60 data points, respectively, during the training process of the MLP algorithm in a loop. The best architecture was investigated by changing the radial basis layer neuron number and spread coefficient as a parameter of Radial basis function (RBF). The tests were performed using the a

Table 8 Coefficients of the main proposed correlation (Eq. 9) obtained by ANN analyses

Eq. (9): $h = A(\frac{k_l}{d})(\mathrm{Re}_g)^B(f_{\mathrm{tp}})^C(\mathrm{Fr})^D(x)^E(\mathrm{Bo})^F(\Delta T_{\mathrm{sat}})^G(f_l^2)^H(\mathrm{We})^I(\Delta P\frac{L}{P})^J(\mathrm{Re}_l)^K$

Equations/ coefficients	Eq. (30)	Eq. (31)	Eq. (32)	Eq. (33)	Eq. (34)	Eq. (35)	Eq. (36)	Eq. (37)	Eq. (38)	Eq. (39)
A	60.19365	0.100143	−0.06397	3.327234	3.550174	6.20412	5.867284	21.73028	21.77796	21.70193
B	0.171773	0.516859	0.096179	−0.06397	−0.13991	−1.01466	−1.01955	−0.92148	8.05E-05	8.04E-05
C	0	−0.16681	0.511016	0.096179	0.095697	−0.00078	−0.00017	−0.00024	−0.92141	−0.92182
D	0	0	−0.13459	0.511016	0.090395	1.005651	1.001148	1.003015	−0.00036	−0.00036
E	0	0	0	−0.13459	0.55255	1.165526	1.164891	1.008696	1.003108	1.003111
F	0	0	0	0	−0.11753	−0.081	0.004695	0.002929	1.008488	−0.00047
G	0	0	0	0	0	−1.00624	−0.08187	−0.09576	0.002944	1.009437
H	0	0	0	0	0	0	−1.00106	0.092417	−0.09589	0.002547
I	0	0	0	0	0	0	0	−1.00344	0.092563	−0.09586
J	0	0	0	0	0	0	0	0	−1.00354	0.092303
K	0	0	0	0	0	0	0	0	0	−1.00353

spread coefficient of 100, 1,000, 10,000, 100,000, 1000,000, 10,000,000 and for the radial basis layer 50, 100, 150, 200, 250, 300, 350, 400, 450, 500.

The experimental data include the mass fluxes of 200, 300 and 400 kg m^{-2} s^{-1} belonging to the saturation temperatures of 10, 15 and 20 °C as shown in Table 3 and also in Figs. 5, 6, 7, 8, 9, 10, 11. Table 4 shows the best predictive method for the convective heat transfer coefficient (a) and pressure drop (b) regarding with the several error analysis such as R-square, proportional error and means square error (MSE). The performance of the method of multi-layer perception (MLP) with 10-5-1 architecture and radial basis function networks (RBFN) with the spread coefficient (sp) of 100,000 and hidden layer neuron number of 200, shown in Table 4, were found to be superior to other methods and architectures by means of satisfactory results with their deviations within the range of ±0.001677 % for the estimated pressure drop (Table 4a), and ±0.358 % for the estimated evaporation heat transfer coefficient (Table 4b). In addition to this, according to the evaporation temperatures of 10, 15 and 20 °C, comparison of the experimental heat transfer coefficients and pressure drops with those from various artificial neural network methods of test groups of all the tested tubes are shown in Figs. 5, 6, 7, 8, 9, 10 in a 30 % deviation line for the pressure drop and 5 % deviation line for the evaporation heat transfer coefficient. It can be clearly seen from these figures and tables that the radial basis function networks (RBFN) have poorer predictability of experimental data than the method of multi-layer perceptron (MLP).

In terms of the use of high data numbers for the accuracy and validation process of the experiments, numerical calculations are done by means of 300 experimental data points in all tables and figures. Tables 5, 6, 7 show the dependency of the input parameters on the outputs of the study according

Table 9 Evaluation of proposed correlations of convective heat transfer coefficient obtained from ANN analysis that belong to the all tested tubes according to the error rates for the mass fluxes of 200, 300, 400 kg m^{-2} s^{-1} and T_{sat} = 10, 15 and 20 °C

h (W m^{-2} K^{-1})	Error analysis/ANN methods		
	R square	Proportional (%)	Square law
Eq. (30)	0.536928	4.821048	53,059.02
Eq. (31)	0.766083	3.348161	26,881.77
Eq. (32)	0.852823	2.692073	16,573.89
Eq. (33)	0.8784	2.418055	13,687.29
Eq. (34)	0.901808	2.195584	11,052.15
Eq. (35)	0.999891	0.068428	12.22074
Eq. (36)	0.999952	0.040852	5.360154
Eq. (37)	0.99997	0.034258	3.372134
Eq. (38)	0.99997	0.034129	3.364506
Eq. (39)	0.99997	0.034181	3.361205

to the error rates of the test group of ANN, as a result of the most predictive ANN method of the MLP 10-5-1 architecture for the mass fluxes of 200, 300, 400 kg m^{-2} s^{-1} and evaporation temperatures of 10, 15 and 20 °C. They also show the most predictive combinations of input parameters, whose deviations are over 0.5 %, according to the error rates for the determination of evaporation heat transfer coefficient (h) and pressure drop (ΔP). The input parameters are shown with numbers in these tables as follows: average vapour quality (I), mass flux (II), evaporating temperature (III), heat flux (IV), depth of corrugation (V), helix angle of corrugation (VI), two-phase friction factor (VII), Bond number (VIII), liquid Reynolds number (IX), vapour Reynolds number (X), two–phase multiplier (XI), Froude number (XII),Weber number (XIII) and temperature difference between the tube wall and

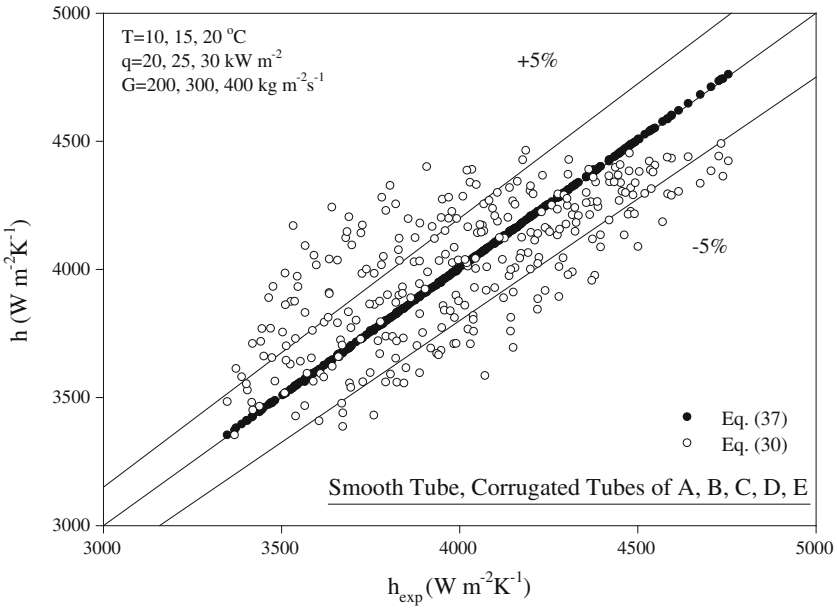

Fig. 11 Comparisons of experimental convective heat transfer coefficients (**b**) with the proposed empirical correlations by artificial neural network methods for all tubes

saturation temperature (XIV). Table 5 shows each input parameter's predictability of the outputs of experimental pressure drop and evaporating heat transfer coefficient separately. They are ordered from the best predictive to the worst predictive one in all tables considering the experimental pressure drop. For instance, artificial intelligence was able to determine the experimental pressure drop and evaporation heat transfer coefficient with an accuracy of over 74 % by means of the separate use of inputs of vapour Reynolds number (X), Froude number (XII) and Weber number (XIII) in Table 5. In Tables 6 and 7, neural network analyses tried to determine the outputs by means of two and three known input combinations. Prediction rates on these tables increase with increasing added input numbers due to the result of the learning process of the artificial intelligence. For example, when the helix angle of corrugation (VI) and two-phase friction factor (VII) are selected as known inputs in Table 6, their predictabilities are found as 78.2 and 80 % for the outputs of pressure drop and heat transfer coefficient, respectively. In Table 7, when the vapour Reynolds number (X) is added to the selected inputs of the helix angle of corrugation (VI) and two-phase friction factor (VII), the prediction rate increases to 98.6 % for the pressure drop and 95.2 % for the evaporating heat transfer coefficient in comparison with the former situation. As a result, it is possible to derive many results from these figures on the input combination performance. For another example, it should be noted that in spite of the rather low self-prediction rate of two-phase friction factor (IV) in Table 5, it produced a good combination with others and increased the predictability in these tables.

The correlation development study results are shown in Tables 8 and 9, and also in Fig. 11. The main frame of the proposed correlation is shown in Eq. (9) which has 12 possible dominant parameters on the evaporation heat transfer coefficient. Artificial intelligence decided the coefficients of these significant parameters step by step in Table 8 and their error rates can be seen in Table 9. It is possible to see the success of each term in Eq. (9) in this table. It also shows that the accuracy of the estimated output values by means of added input values increases with increasing added proper input parameters into Eq. (9). Equation (30) is found to have the lowest predictability, while Eq. (37) has the optimum predictability in Table 9 and their performance comparison is shown in Fig. 11. The majority of the data obtained from the ANN analysis of Eq. (30) fall between the deviations of ±5 % in this figure. It can be seen that Eq. (37) showed a great success with its accuracy in Fig. 11.

A large number of graphics could be generated from the output of the calculations; however, due to space limitation only the typical results are shown from the experimental database of the authors. It should also be noted that detailed information on the evaporation heat transfer characteristics of the study with some additional figures and different experimental parameters can be seen in the authors' previous publications.

5 Conclusion

Comparison of the numerical evaporation heat transfer coefficient and pressure drop values with the measured values by means of artificial intelligence methods was performed in this paper. There is no research on the content of this paper considering its parameters in current literature. The results of this study are expected to fill this gap in the literature.

Except for the different architectures of the artificial neural network (ANN) methods of multi-layer perceptron (MLP)

and radial basis networks (RBFN), the performance of the method of MLP with 10-5-1 architecture and RBFN with the spread coefficient of 100,000 are found to be capable of predicting the evaporation heat transfer coefficient and pressure drop of R134a in a vertical tube within the range of ±30 % and also within very small error rates.

Convective heat transfer coefficient and pressure drop of R134a in the paper are found to be dependent on mass flux, heat flux, the temperature difference between the tube wall and saturation temperature, average vapour quality, evaporating temperature, two-phase friction factor, two-phase multiplier, liquid and vapour Reynolds numbers, Bond number, Froude number, Weber number, depth of corrugation and helix angle for the tested corrugated tubes according to the results of the analysis.

The new empirical correlations, based on this simple architecture which have never appeared in the literature, for predicting the convective heat transfer coefficient valid for the evaporation process in a smooth tube and five different corrugated tubes, are proposed for practical applications.

Acknowledgments The first author wishes to thank King Mongkut's University of Technology Thonburi (KMUTT) for providing him with a Post-doctoral fellowship. The third and fourth authors wish to thank the Thailand Research Fund, the Office of the Higher Education Commission and the National Research University Project for financial support for this study.

References

1. Nozu, S.; Honda, H.; Nakata, H.: Condensation of refrigerants CFC11 and CFC113 in the annulus of a double-tube coil with an enhanced inner tube. Exp. Therm. Fluid Sci. **11**, 40–51 (1995)
2. Nozu, S.; Honda, H.; Nishida, S.: Condensation of a zeotropic CFC 114-CFC 113 refrigerant mixture in the annulus of a double-tube coil with an enhanced inner tube. Exp. Therm. Fluid Sci. **11**, 364–371 (1995)
3. Dong, Y.; Huixiong, L.; Tingkuan, C.: Pressure drop, heat transfer and performance of single-phase turbulent flow in spirally corrugated tubes. Exp. Therm. Fluid Sci. **24**, 131–138 (2001)
4. Zimparov, V.: Enhancement of heat transfer by a combination of three-start spirally corrugated tubes with a twisted tape. Intern. J. Heat Mass Transf. **44**, 551–574 (2001)
5. Zimparov, V.: Enhancement of heat transfer by a combination of a single-start spirally corrugated tubes with a twisted tape. Exp. Therm. Fluid Sci. **25**, 535–546 (2002)
6. Zimparov, V.: Prediction of friction factors and heat transfer coefficients for turbulent flow in corrugated tubes combined with twisted tape inserts. Part 1: friction factors. Intern. J. Heat Mass Transf. **47**, 589–599 (2004)
7. Zimparov, V.: Prediction of friction factors and heat transfer coefficients for turbulent flow in corrugated tubes combined with twisted tape inserts. Part 2: heat transfer coefficients. Intern. J. Heat Mass Transf. **47**, 385–393 (2004)
8. Nafey, A.S.: Neural network based correlation for critical heat flux in steam-water flows in pipes. Intern. J. Therm. Sci. **48**, 2264–2270 (2009)
9. Wang, W.J.; Zhao, L.X.; Chun-Lu, Z.: Generalized neural network correlation for flow boiling heat transfer of R22 and its alternative refrigerants inside horizontal smooth tubes. Intern. J. Heat Mass Transf. **49**, 2458–2465 (2006)
10. Scalabrin, G.; Condosta, M.; Marchi, P.: Mixtures flow boiling: modeling heat transfer through artificial neural networks. Intern. J. Therm. Sci. **45**, 664–680 (2006)
11. Scalabrin, G.; Condosta, M.; Marchi, P.: Modeling flow boiling heat transfer of pure fluids through artificial neural networks. Intern. J. Therm. Sci. **45**, 643–663 (2006)
12. Wongwises, S.; Disawas, S.: Two-phase evaporative heat transfer coefficients of refrigerant HFC-134a under forced flow conditions in a small horizontal smooth tube. Intern. Commun. Heat Mass Transf. **27**, 35–48 (2000)
13. Sripattrapan, W.; Wongwises, S.: Two-phase flow of refrigerants during evaporation under constant heat flux in a horizontal tube. Intern. Commun. Heat Mass Transf. **32**, 386–402 (2005)
14. Wongwises, S.; Polsongkram, M.: Evaporation heat transfer and pressure drop of HFC-134a in a helically coiled concentric tube-in-tube heat exchanger. Intern. J. Heat Mass Transf. **49**, 658–670 (2006)
15. Kaew–On, J.; Wongwises, S.: Experimental investigation of evaporation heat transfer coefficient and pressure drop of R-410A in a multiport mini-channel. Intern. J. Ref. **32**, 124–137 (2009)
16. Posew, K.; Laohalertdecha, S.; Wongwises, S.: Evaporation heat transfer enhancement of R-134a flowing inside smooth and microfin tubes using the electrohydrodynamic technique. Energy Conv. Manag. **50**, 1851–1861 (2009)
17. Laohalertdecha, S.; Wongwises, S.: An experimental study into the evaporation heat transfer and flow characteristics of R-134a refrigerant flowing through corrugated tubes. Intern. J. Ref. **34**, 280–291 (2011)
18. Aroonrat, K.; Wongwises, S.: Evaporation heat transfer and friction characteristics of R-134a flowing downward in a vertical corrugated tube. Exp. Therm. Fluid Sci. **35**, 20–28 (2011)
19. Balcilar, M.; Dalkilic, A.S.; Wongwises, S.: Artificial neural network techniques for the determination of condensation heat transfer characteristics during downward annular flow of R134a inside a vertical smooth tube. Intern. Commun. Heat Mass Transf. **38**, 75–84 (2011)
20. Colorado, D.; Ali, M.E.; Garcia-Valladares, O.; Hernandez, J.A.: Heat transfer using a correlation by neural network for natural convection from vertical helical coil in oil and glycerol/water solution. Energy **36**, 854–863 (2011)
21. Fausett, L.: Fundamentals of neural networks, architectures, algorithms, and applications, Prentice-Hall, Inc. Press, Prentice–Hall (1994)
22. Matlab, R2010a, 2010, http://mathworks.com/
23. Dittus, F.W.; Boelter, L.M.E.: Engineering publication, vol. 2, p. 443, University of California, California (1930)
24. Zivi, S.M.: Estimation of steady-state steam void-fraction by means of the principle of minimum entropy production. Trans. ASME J. Heat Transf. Ser. C **86**, 247–252 (1975)
25. Chisholm, D.: Pressure gradients due to friction during the flow of evaporating two-phase mixtures in smooth tubes and channels. Intern. J. Heat Mass Transf. **16**, 347–358 (1973)
26. Duda, R.O.; Hard, P.E.; Stork, D.G.: Pattern classification (2nd Edn). Wiley, New York (2002)